CAMBRIDGE
UNIVERSITY PRESS

Article

Evidence of fluid-induced myrmekite formation after alkali-feldspar megacrysts: an example from a meta-porphyritic granitoid in Makrohar, Madhya Pradesh, India

Arimita Chakrabarty[1], Shreya Karmakar[2], Upama Dutta[3] , Sanjoy Sanyal[1] and Pulak Sengupta[1]

[1]Department of Geological Sciences, Jadavpur University, Kolkata 700032, India; [2]Department of Earth and Environmental Studies, National Institute of Technology (NIT), Durgapur 713209, India; and [3]Department of Applied Geology, Indian Institute of Technology (Indian School of Mines), Dhanbad 826004, India

Abstract

A meta-porphyritic granitoid in the Makrohar Granulite Belt, Central India contains extensive myrmekite. This work evaluates the controls of fluid in relation to deformation and the formation of myrmekite all along the periphery of an alkali-feldspar megacryst. Two different myrmekite morphologies are present: (1) vermicular intergrowth of plagioclase (An_{38-39}) and quartz (Myr1); and (2) polygonal aggregates of coarse plagioclase (An_{45-46}) and quartz (Myr2). Petrographic features suggest that myrmekite Myr1 nucleates on alkali-feldspar and plagioclase porphyroclasts and the myrmekite front moved into the alkali feldspar by replacing it; and that myrmekite Myr2 and the secondary biotite which replaces plagioclase porphyroclasts and garnet form together. Deformation had a decisive role in forming the polygonal aggregates of Myr2, however field and microtextural features do not support any significant control of deformation during the formation of Myr1. Reaction modelling and a mass-balance calculation suggest that Ca and Na are added to, and K is removed from, the alkali feldspar during the myrmekite formation at nearly constant Si and Al. However, the secondary biotite-forming reaction, consumes K and releases Ca. Interpretation of the reaction textures in different isothermal–isobaric sections of $\mu K_2O–\mu CaO$ in the KCFASH system suggest that CaO and K_2O moved in opposite directions for myrmekitisation and along their respective chemical potential gradients created between the sites of formation of myrmekite and secondary biotite. The feedback mechanism which operated between the two reaction sites was controlled by infiltration of brine-rich fluid in the meta-granitoid during a regional hydration event (550–600°C and 5–6 kbar). Volume reduction of ~10% during the formation Myr1 and Myr2 drew the brine-rich fluid towards the alkali feldspar and thus facilitated the process of myrmekite formation. Variation in the morphology of quartz in the myrmekite is attributed to the cooling of the complex.

Keywords: myrmekite; deformation; metasomatism; fluid infiltration; chemical potential

Introduction

The origin of the delicate intergrowth of quartz rods with plagioclase that was first identified in 1879 by F. Fouqué and A. Michel-Lévy (Fouqué and Michel-Lévy, 1879) as 'vermicular quartz' and was given the name 'myrmekite' by Sederholm (1899) remains elusive to this day. More than a century ago, two hypotheses were proposed to explain myrmekite on alkali feldspar. Becke (1908) considered that myrmekite forms by replacement of the immediate alkali feldspar due to fluid-induced Ca and Na alteration of the latter (the 'replacement' theory). Whereas Schwantke (1909) proposed that plagioclase and quartz in the myrmekite were derived from the immediate alkali feldspar (the 'exsolution' theory). A detailed investigation by Ashworth (1972) argued that both the earlier processes, i.e. replacement and exsolution, can operate simultaneously at constant Al and

Si during the formation of myrmekite on alkali feldspar. A review of myrmekite research until the end of 1970s is given by Phillips (1980). Myrmekite that develops preferentially on alkali feldspar (rarely on albitic plagioclase, Ashworth, 1986), is reported from highly deformed as well as weakly deformed rocks of diverse lithologies (Cisneros-Lazaro *et al.*, 2019; Ceccato *et al.*, 2018; Abart *et al.*, 2014; Cesare *et al.*, 2002; Vernon *et al.*, 1983; Tsurumi *et al.*, 2002). A majority of the studies post 1980 support the Becke (1908) replacement theory to be the dominant chemical process in the myrmekite formation, though the control of deformation in the process remains a debated topic (reviewed in Vernon, 2004; Menegon *et al.*, 2006; Abart *et al.*, 2014; Cisneros-Lazaro *et al.*, 2019). Features such as restriction of myrmekite to surfaces of deformed alkali feldspar with high elastic strain and the large negative volume change of the myrmekite-forming reactions (up to 10 vol.%, Simpson and Wintsch, 1989) are cited as evidence in support of the control of deformation on the growth of myrmekite (Simpson and Wintsch, 1989). Vernon *et al.* (1991), in contrast, argued that deformation only helps the access of Ca-, Na-bearing fluid to alkali feldspar and hence, is not the essential condition for myrmekite formation.

Extensive development of myrmekite all along the periphery of the alkali feldspar in a contact metamorphosed granite (Cesare *et al.*, 2002), granite mylonite (Menegon *et al.*, 2006) and in undeformed granite (Abart *et al.*, 2014) suggests that fluid exerted a strong control and can even overpower the effect of stress. Irrespective of the role of deformation, the fact remains that the formation of myrmekite requires chemical alteration of alkali feldspar in an open system, at least on the scale of myrmekite formation. For the myrmekite-forming process to progress significantly low chemical potentials for Ca and Na (high chemical potential for K) have to be maintained at the alkali-feldspar site to enable the transport of Ca and Na towards (and removal of K from) the myrmekite front. Some studies invoke destabilisation of plagioclase by secondary hydrous phases as a source for Ca and Na for myrmekite formation (Simpson and Wintsch, 1989). However, no detailed study has been published that explains how the chemical potential gradients that drive the transport of Ca and Na towards and K away from the myrmekite front were created and maintained during the formation of myrmekite. A number of studies have demonstrated that Al and Si can be substantially mobile during fluid–rock interaction (reviewed in Philpotts and Ague, 2009). Hence, any assumption of constancy of Al and Si in the myrmekite forming process needs to be studied on case by case basis.

In this communication we describe extensive development of myrmekite on all sides of alkali feldspar in a weakly deformed meta-porphyritic granitoid from the Makrohar Granulite Belt of the Central Indian Tectonic Zone. By interpreting the field and petrological observations in different isothermal–isobaric chemical potential diagrams and a textural modelling study, it is demonstrated that the myrmekite-forming reaction was coupled with the reaction that formed secondary biotite after plagioclase and garnet in the vicinity. The two reactions generated low chemical potentials of CaO and K_2O at the sites of secondary biotite and the myrmekite front, respectively. Consequently CaO and K_2O moved along its respective lower chemical potential and caused extensive development of myrmekite on all sides of the alkali-feldspar porphyroclasts of different dimensions. Aluminium and Si remained conserved during the chemical alteration process. This study demonstrates that pervasive infiltration of fluid, presumably brine, in a large volume of the rock, acted as a carrier and helped the transport of CaO and K_2O in the reverse direction. The influence of pressure, temperature and deformation on the myrmekite-forming process is discussed.

Geological background

Dissecting the Archean–early Paleoproterozoic crust of the Indian shield, the ENE–WSW trending fold belt, commonly known as Central Indian Tectonic Zone, preserves more than 1 billion year of Earth's history from ~2.1 Ga to 0.9 Ga (Fig. 1a, reviewed in Chattopadhyay *et al.*, 2020, Chakrabarty *et al.*, 2022). There is a general consensus that the Central Indian Tectonic Zone has stitched together the northern (Aravalli–Bundelkhand craton) and the southern (Bastar, Singhbhum and Dharwar craton) blocks of the Archean/early Paleoproterozoic and contains the protracted geological history of magmatism, sedimentation and metamorphism that are linked to the two supercontinental cycles, namely Columbia and Rodinia (Chattopadhyay *et al.*, 2020). The Central Indian Tectonic Zone exposes three distinct granulite belts: Makrohar to the northeast and Ramakona–Katangi and Balaghat–Bhandara to the south. Only the studied Makrohar

granulite belt, the northeast part of the Central Indian Tectonic Zone is shown in Fig. 1b. The geological and geochronological attributes of the Central Indian Tectonic Zone are discussed in detail in a number of publications (Bhowmik, 2019; Chattopadhyay *et al.*, 2020) and will not be repeated here. The area studied that is a part of the Makrohar granulite belt is constituted predominantly of three lithological units with distinct petrological and geochronological characteristics (Fig. 1c and reviewed in Chakrabarty *et al.*, 2022, 2023). The oldest unit is a suite of granitoids that commonly preserves euhedral and subhedral feldspar in a fine-grained matrix, and are variably deformed and metamorphosed (hereafter the meta-porphyritic granitoids, reviewed in Chakrabarty *et al.*, 2023). The meta-porphyritic granitoids, the major rock type of the area studied (Fig. 1c), have bulk compositions which resemble those of I-type granitoids of continental arc settings (Chakrabarty *et al.*, 2023). The *in situ* U–Pb radiometric age of zircon indicates that the magmatic protolith of the meta-porphyritic granitoids was emplaced at ~1.75 Ga (Chakrabarty *et al.*, 2023). A suite of felsic orthogneisses whose magmatic protolith was formed during 1.4–1.35 Ga (confirmed by U–Pb zircon age determination) and which intruded the magmatic protolith of the meta-porphyritic rocks (Chakrabarty *et al.*, 2022) is the second major lithounit of the area (Fig. 1c). An ensemble of meta-supracrustal rocks consisting of meta-pelites/psammopelites, marble and calc-silicate rocks represent the third lithological unit of the area. As a consequence of extensive tropical weathering the relations between the meta-supracrustal rocks with the other lithologies can not be established with confidence. Nevertheless, isolated patches of the metamorphosed supracrustal rocks of different dimensions are surrounded by the meta-porphyritic rocks (Fig. 1c). Nowhere in the area do the meta-porphyritic rocks cross-cut the members of meta-supracrustal rocks (Karmakar, 2021, Chakrabarty *et al.*, 2022, 2023). The field features are consistent with the view that the sedimentary protolith of the meta-supracrustal rocks were deposited on the magmatic protolith of the meta-porphyritic granitoids (Chakrabarty *et al.*, 2022). No direct contact between the felsic orthogneisses and the meta-supracrustal rocks has been seen. All the lithological units are deformed intensely and metamorphosed at c. 0.95 Ga (Chakrabarty *et al.*, 2022). The deformation is manifested by coaxial superposed folding of mafic dykes, compositional banding in meta-supracrustal rocks and the gneissic banding of the felsic orthogneisses (Karmakar 2021, Chakrabarty *et al.*, 2022). Euhedral to subhedral feldspars in the meta-porphyritic rocks are stretched, in places (feldspar augen) parallel to the regional planar fabric developed in other lithologies including the felsic orthogneisses and meta-supracrustal rocks (Chakrabarty *et al.*, 2022). The metamorphism culminated at 800–850°C at 7–7.5 kbar and was followed successively by a steeply decompressive and near isobaric retrograde P–T path that is common in a continent–continent collision setting (Chakrabarty *et al.*, 2022). The near isobaric cooling path that spans over ~550±50°C and ~5±1 kbar is accompanied by infiltration-driven metamorphism in all the lithologies (reviewed in Chakrabarty *et al.*, 2022). Studies of Karmakar (2021) and Chakrabarty *et al.* (2022, 2023) show that these infiltration-driven metamorphism events caused variable hydration of the granulite-facies assemblage in the felsic orthogneisses (formation of secondary amphibole and biotite after orthopyroxene), marble and calc-silicate rocks (development of clinohumite), meta-porphyritic granitoid (development of biotite foliation) and olivine norite (amphibole, biotite after olivine, clinopyroxene and plagioclase). The c. 0.95 Ga tectonothermal events that are recorded in this study
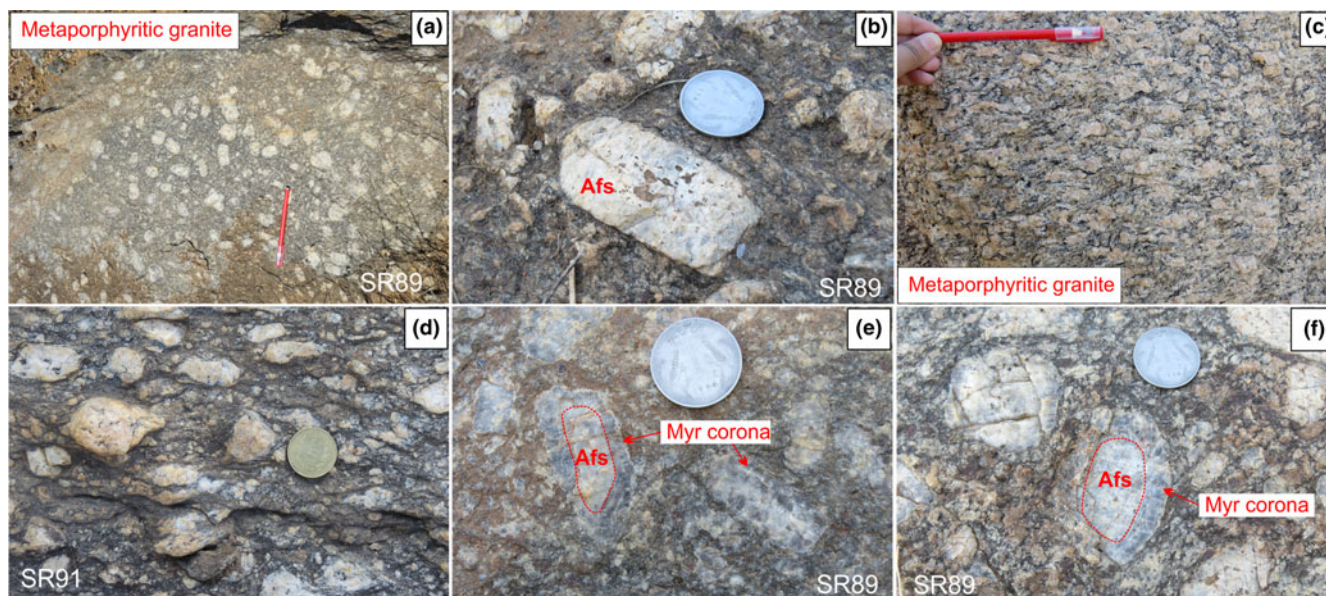
Figure 1. (a) The geological map of the Peninsular and Extra-peninsular India showing different components (Central Indian Tectonic Zone is marked in a light yellow colour) (modified after Chakrabarty *et al.*, 2023). The red box area contains parts of the Son-Valley Vindhyan sediments, Mahakoshal Group of rocks, Makrohar Granulite Belt and Gondwana Supergroup (sedimentary rocks). (b) The enlarged map of the red squared area of Fig. 1a; modified after Chakrabarty *et al.* (2022, 2023). The study area is marked with a red rectangle that is a part of the Makrohar Granulite Belt. (c) Enlarged lithological map of the study area, comprising four major lithounits. Foliation in felsic orthogneiss and meta-porphyritic granitoids give the regional planar fabric, defined by gneissic banding and stretched feldspars, and matrix biotite foliation, respectively. Sample locations are marked (red stars).

seem to be the most pervasive event in the entire Central Indian Tectonic Zone (reviewed in Chattopadhyay *et al.*, 2020; Bhowmik, 2019; Chakrabarty *et al.*, 2022).

Field features

A detailed field description of the meta-porphyritic rock studied is given in Chakrabarty *et al.* (2023). In the following section only the salient features related to theme of the present communication are presented below.

The meta-porphyritic granitoids, in most places, show no strong influences of deformation at the outcrop scale. The rock has randomly oriented subhedral-to-euhedral plagioclase (2–3 cm length and width) and alkali feldspar (7–8 cm in length, 3–5 cm in width; locally with Carlsbad twinning) megacrysts that are set in a distinctly finer grained matrix (Fig. 2a–c). The matrix

consists of feldspars, quartz, garnet, biotite with minor ilmenite. Significant variations in terms of porphyroclast–matrix ratio, aspect ratio and modal proportion of the feldspar megacrysts are present (Chakrabarty *et al.*, 2023). In the relatively deformed part, feldspar porphyroclasts have elliptical-to-sub-elliptical habits (hereafter feldspar augen) with thin and laterally continuous-to-discontinuous foliation of biotite swerving around them (Fig. 2d). The feldspar augen show no deflection of the tapered end (i.e. no σ or δ kinematic indicative tails have formed), nor any distinct lineation. Combining these features; the presence of abundant euhedral crystals of megacryst feldspar and the absence of intense grain-size reduction in laterally persistent zones, it can be stated that the meta-granitoids studied are not mylonites (Vernon, 2004, p. 486). The regional deformation pattern corroborates this view (Chakrabarty *et al.*, 2022). The laterally discontinuous biotite foliation is sparsely developed in the less deformed

Figure 2. Field features of meta-porphyritic granitoids. Mineral abbreviations are after Whitney and Evans (2010). (a) Matrix-dominated (clast:matrix = 1:2) meta-porphyritic granitoid in which feldspar porphyroclasts are scattered within a fine-grained dark matrix, consisting of biotite, garnet, quartz and feldspar. (b) Idiomorphic tabular alkali-feldspar megacryst. (c) Clast-dominated meta-porphyritic granitoid (clast:matrix = 3:1) where fine grained, mostly aligned biotite-enriched matrix swerves around rounded pink feldspar phenocrysts. (d) At a few locations, deformation signatures are preserved by feldspar augen and alignment of matrix biotite. (e,f) Dark translucent corona surrounds the milky white core of an alkali-feldspar megacryst.

part of the meta-porphyritic rock. Randomly oriented alkali-feldspar megacrysts with both euhedral-to-elliptical outlines are completely surrounded by a grey, translucent rim that resembles 'rapakivi' texture (Fig. 2e,f). Optical and scanning electron microscopy conform that the grey, translucent rim is an inter-growth of quartz–plagioclase i.e. myrmekite. The thickness of the myrmekite rim is not constant and varies along the periphery of a single grain as well as between grains.

Materials and methods

Petrographic studies of polished sections (27×46 mm) and larger thin sections (50×75 mm) were undertaken by optical petography and scanning electron microscopy (SEM). Comparatively small alkali-feldspar phenocrysts, representative of the megacrysts were selected for mineral compositional analysis. Back-scattered electron (BSE) images were taken using a ZEISS EVO-18 SEM at Jadavpur University, Kolkata, India, equipped with an energy dispersive spectrometer (EDS), operating at an accelerating voltage of 20 kV and a beam current of 1.0 nA.

Compositions of the minerals were determined with a CAMECA SX5 microprobe with 5 wavelength dispersive spectrometers (WDS) at the Central Research Facility of the Indian Institute of Technology (IIT-ISM), Dhanbad. Operating conditions were 15 kV accelerating voltage and 15 nA beam current, with a beam diameter of 2–3 μm. Natural standards were used for most major elements (Si, Al, Cr, Fe, Mg, Ca, Na and K) except for Mn and Ti, for which synthetic standards were used. The measured compositions and calculated cations per formulae unit of representative minerals are presented in Supplementary table 1a–c. Mineral abbreviations in all the figures and tables are after Whitney and Evans (2010).

In order to obtain balanced chemical reactions from the measured compositions of the minerals conforming to textural relations (textural modelling study), the Singular Value

Decomposition (SVD) technique has been used (Lang *et al.*, 2004; Roy Choudhury *et al.*, 2023; Chatterjee *et al.*, 2022). The computer program *C-space* which employs the condition of mass balance and solves linear algebraic equations following the SVD technique has been used following the procedures presented in Torres-Roldan *et al.* (2000). The detailed procedure of the textural modelling study that integrates measured phase compositions and the observed textures are described at length in several studies e.g. Lang *et al.* (2004), Chowdhury *et al.* (2013), Karmakar *et al.* (2017) and Yuguchi *et al.* (2015, 2019, 2022). Representative mineral compositions used for *C-space* modelling are listed in Supplementary table 1a–c. To calculate the volume change for solid phases (ΔV_S) of a balanced chemical reaction, the following methods are used: first, the amount (mole), expressed as coefficients of each solid phase in the balanced chemical reaction are multiplied with the respective molar volume of the phase. ΔV_S of the reaction is then calculated from the total volume of the product side and the total volume of the reactant side for the solid phases only. The molar volumes of the required phases are taken from the internally consistent thermodynamic dataset (hp02ver) by Holland and Powell (1998) using the computer program *PERPLE_X* (6.9.1) (Connolly, 2005, 2009) at the estimated *P–T* condition. The isothermal–isobaric chemical potential (μ) diagrams are computed in the KCFASH system using the updated version of *PERPLE_X* (6.9.1) and the internally consistent thermodynamic dataset of Holland and Powell. The activities of the solid-solution phases are calculated from the measured phase compositions using the *A-X* program of Holland and Powell (2009).

Results

Petrography

Because of the large grain size of the meta-porphyritic rock (Fig. 2a), mutual relations between the different minerals render petrography study difficult. Nevertheless, optical and BSE images

provide information on the spatial and temporal relations of quartz–plagioclase intergrowths (myrmekite) with other minerals. A general description of the textural relations of the rock is given in Chakrabarty *et al.* (2023). Only those features that are related to the formation of myrmekite are described below.

Texture and microstructure of the meta-porphyritic granitoid
Optical and BSE images, show that alkali feldspar and plagioclase are present in the megacryst and in the matrix. The presence of complex twining and oscillatory zoning in plagioclase (Fig. 3a, b), relict tartan twins in alkali feldspar (Fig. 3c) and the euhedral habit of the feldspar megacryst in less-deformed rocks are interpreted as evidence of the magmatic crystallisation of the feldspars (Chakrabarty *et al.*, 2023). Alkali-feldspar megacrysts contain inclusions of plagioclase and quartz and locally develop very fine-grained plagioclase lamellae (Fig. 3d,e). Commonly, the magmatic feldspars show evidence of deformation with the intensity of rock deformation varying significantly from weakly deformed to relatively more deformed. This is manifested by bending of the lamellar twin planes of plagioclase, undulose extinction, grain-boundary recrystallisation and formation of polygonal aggregates along the margins of feldspar (Fig. 3a, f–h). Recrystallisation is more pronounced in the alkali feldspar than the plagioclase grains. The deformed feldspar grains, megacrysts and those in the matrix, will be referred to as feldspar porphyroclasts. In the relatively deformed part of the rock, quartz grains in the matrix either form polygonal grain aggregates or form elongate aggregates of coarsely recrystallised grains with planar contacts (Fig. 3h). Grain-boundary bulging of recrystallised quartz are also noted (Fig. 3h). Locally, elongated quartz grains separate the porphyroclasts of plagioclase from alkali feldspar and also form veins within the porphyroclasts of feldspars (Fig. 3i). Garnet with subhedral-to-euhedral outlines are restricted to the matrix. Garnet contains tiny inclusions of ilmenite, quartz, plagioclase and biotite, and are extensively fractured (Fig. 3j). The replacement of garnet by biotite makes estimation of the garnet mode difficult. The preserved garnet portion occupies ~5–10 vol.% of the rock. Biotite occurs in at least four distinct textural modes. The biotite inclusions in garnet are the earliest variety. Biotite with undulose extinction and bending define the biotite foliation that swerves around and replaces garnet and porphyroclasts of feldspar (Fig. 3k). Commonly, the third type of biotite in the foliation have random orientations and lack internal deformation (Fig. 3g). This biotite extensively replaces plagioclase (less commonly the alkali feldspar) and garnet along the grain boundaries and along the fractures. Biotite–quartz intergrowths, in the fourth type, occur randomly and replace feldspars and polygonal aggregates of quartz and plagioclase (Fig. 3l). On the basis of petrographic features, the second to fourth varieties of biotite will be referred to as 'secondary' biotite, because these replace deformed feldspar and garnet grains. The textural/microstructural features also suggest that second to fourth generations of biotite grew during, and outlasted, the deformation that affected the meta-porphyritic rock. Commonly, the plagioclase proximal to the secondary biotite have normal zoning and the thickness of the albitic rim is highly variable. Rarely, the plagioclase with oscillatory zoning have also undergone recrystallisation (Fig. 3b). The dark translucent rims surrounding the alkali-feldspar phenocrysts, as observed in the field, are actually microscopic intergrowths of vermicular and/or polygonal aggregates of quartz + plagioclase (myrmekite), with the details of their microstructure described below.

Textural relations of the myrmekite domains
We define 'myrmekite' as an intimate intergrowth between quartz and plagioclase. The boundary between the myrmekite and the alkali feldspar will be referred to as a 'myrmekite front' and two types of myrmekite, Myr1 and Myr2 are identified, on the basis of morphology. The quartz grains in Myr1 form vermicular intergrowths on a base of plagioclase (Fig. 4a–c). The thickness and the interlamellar distance of quartz show systematic variations. At the immediate contact with the alkali feldspar, quartz vermiculae in Myr1 are thin (20 μm in length and 5 μm in width), have small interlamellar distances (10 μm) and are parallel (Fig. 4a,c). The interface between the small quartz vermiculae and the base plagioclase is slightly curved. The thickness and the interlamellar distance of the quartz vermiculae increase, typically quite abruptly, away from the myrmekite front (Fig. 4a–c). The morphology of these quartz vermiculae are irregular and resemble the 'garben structure' of quartz vermiculae as described by Remmert *et al.* (2018). The myrmekite front has a bulbous shape that is convex towards the alkali feldspar (Fig. 4a,c). The smaller quartz vermiculae are always nearly normal to the myrmekite interface (Fig. 4a–c). In common with the myrmekite around the alkali-feldspar megacrysts (Fig. 2e,f in field features), the shape of the myrmekite front is highly irregular and develops all along the periphery of the smaller alkali-feldspar (Fig. 4d,e). In most places, the myrmekite front dissects the alkali-feldspar. Rafts of alkali feldspar with highly irregular grain boundaries occur in Myr1 (Fig. 4f). Myr1 also develops at the interface of plagioclase inclusions within alkali feldspar (Fig. 4g). The proportion of quartz in Myr1 varies between 20–25 vol.% with the quartz proportion increasing away from the alkali feldspar. In contrast to Myr1, Myr2 are polygonal aggregates, commonly with triple point junctions, and with a size that is distinctly larger (20–40 μm in length and width) than the quartz in Myr1 (Fig. 4h). Commonly, Myr1 forms near the alkali feldspar whereas the Myr2 in the same myrmekite is developed in the distal part that is in contact with plagioclase (Fig. 4h). Direct contact between Myr2 and alkali feldspar is also noted (Fig. 4i). The polygonal Myr2, locally grades into the recrystallised plagioclase along the border of plagioclase porphyroclasts. Myr2 never develops at the interface of the plagioclase inclusion within the alkali feldspar. Myrmekite always develops at the contact between plagioclase and alkali feldspar. In many locations, a layer of quartz separates the myrmekite from, and is oriented parallel to, the grain boundary of plagioclase porphyroclasts (Fig. 4j,k). Where the direct contact between Myr1 and a plagioclase porphyroclast exists, the twining in the latter can be traced within the plagioclase base of the myrmekite (Fig. 4l). These features can be best explained by nucleation of the myrmekite on the plagioclase porphyroclasts (Vernon, 2004; Vernon, 1991; Abart *et al.*, 2012, 2014; Cisneros-Lazaro *et al.*, 2019). The myrmekite forms random veins/apophyses within the alkali feldspar (Fig. 4m). There is an intimate relation between the myrmekite and the secondary biotite. The plagioclase porphyroclasts, typically with normal zoning on which Myr1 and Myr2 grow, are replaced extensively by the secondary biotite. Garnet in the vicinity is also replaced by the secondary biotite. Locally secondary biotite, with or without quartz intergrowths replaces the polygonal aggregates of Myr2, although the immediate Myr1 remains virtually unaffected and has well-defined planar contacts (Fig. 4n,o). Rarely, Myr1 is seen to be replaced by biotite. These textural features support the concept that the bulk of
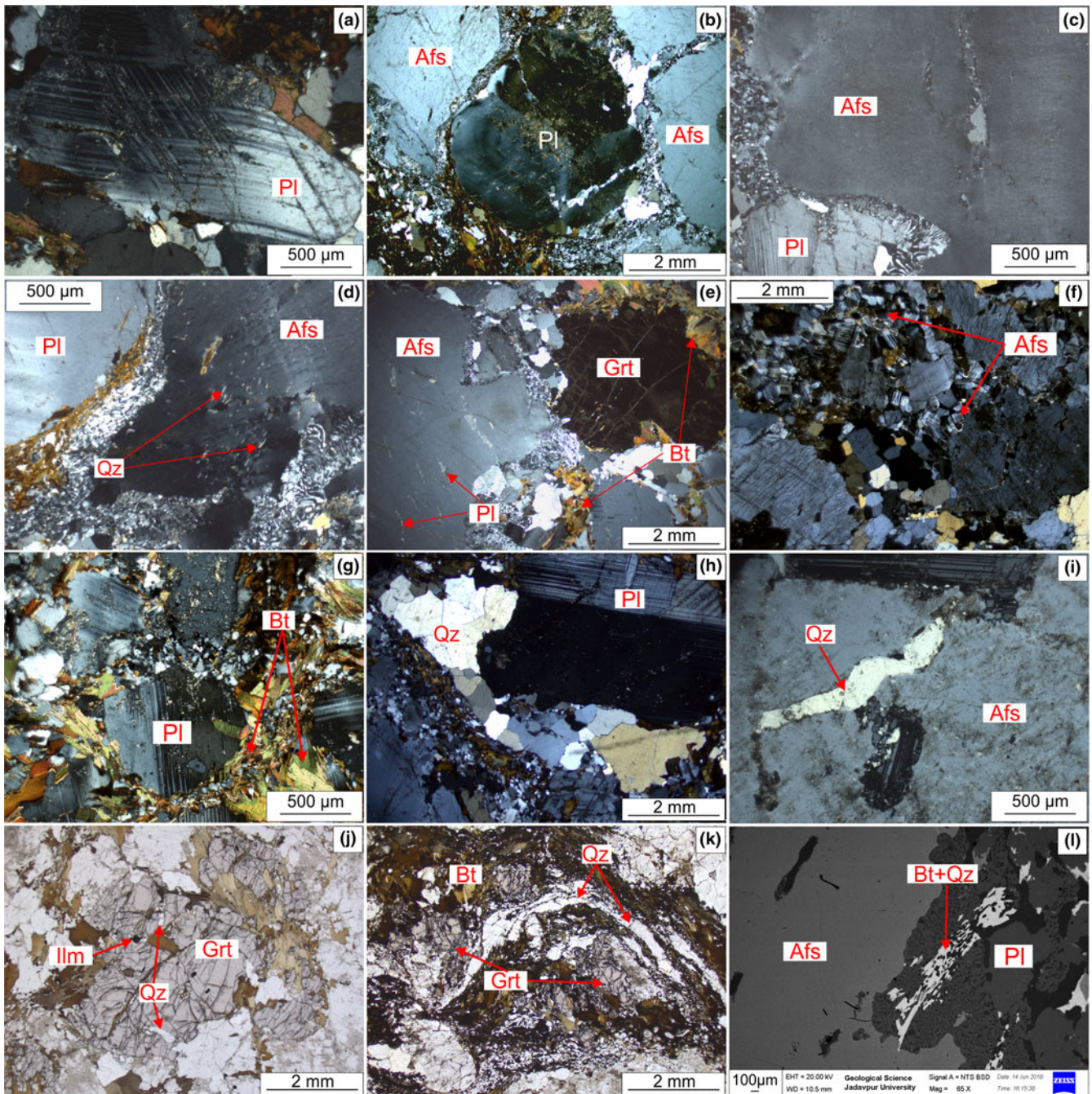
Figure 3. Textural features of the meta-porphyritic granitoid. Mineral abbreviations are after Whitney and Evans (2010). (a) Complex twinning in a plagioclase porphyroclast. (b) Oscillatory zoning and partial recrystallization in a plagioclase porphyroclast. (c) Relict tartan twinning in a alkali-feldspar megacryst. (d) Quartz inclusions in an alkali-feldspar megacryst. Myrmekite and secondary biotite developed in between alkali feldspar and a plagioclase porphyroclast. (e) Very fine plagioclase lamellae within alkali feldspar. Garnet in close proximity to the myrmekite. (f) Fine alkali feldspar in the matrix is extensively recrystallised and exhibits polygonal straight grain boundaries. (g) Polygonal aggregates along the plagioclase boundaries. Biotite in the foliation have random orientations and are free from internal deformation. (h) Grain-boundary bulging of recrystallised quartz along the boundary of a plagioclase porphyroclast. (i) Recrystallised quartz forming veins within the alkali-feldspar porphyroclast. (j) Garnet containing inclusions of ilmenite, quartz, plagioclase and biotite are highly fractured. (k) Biotite with deformation which defines the foliation that swerves around and replaces the garnet, and a feldspar porphyroclast. (l) Biotite–quartz intergrowth replaces a plagioclase porphyroclast together with polygonal aggregates of quartz and plagioclase.

Myr1 was either contemporaneous with or formed after the major part of hydration. Textural features are equivocal regarding the relationships between Myr2 and secondary biotite. The latter can form during, or subsequently to, the deformation producing the polygonal aggregates of quartz and plagioclase. Textural features are also inconclusive regarding the original character of Myr2 prior to recrystallisation. Regardless, the polygonal fabric of Myr2 indicates a reduction of surface energy relative to the vermicular internal texture of Myr1 (cf. Vernon, 2004; Cisneros-Lazaro et al., 2019).
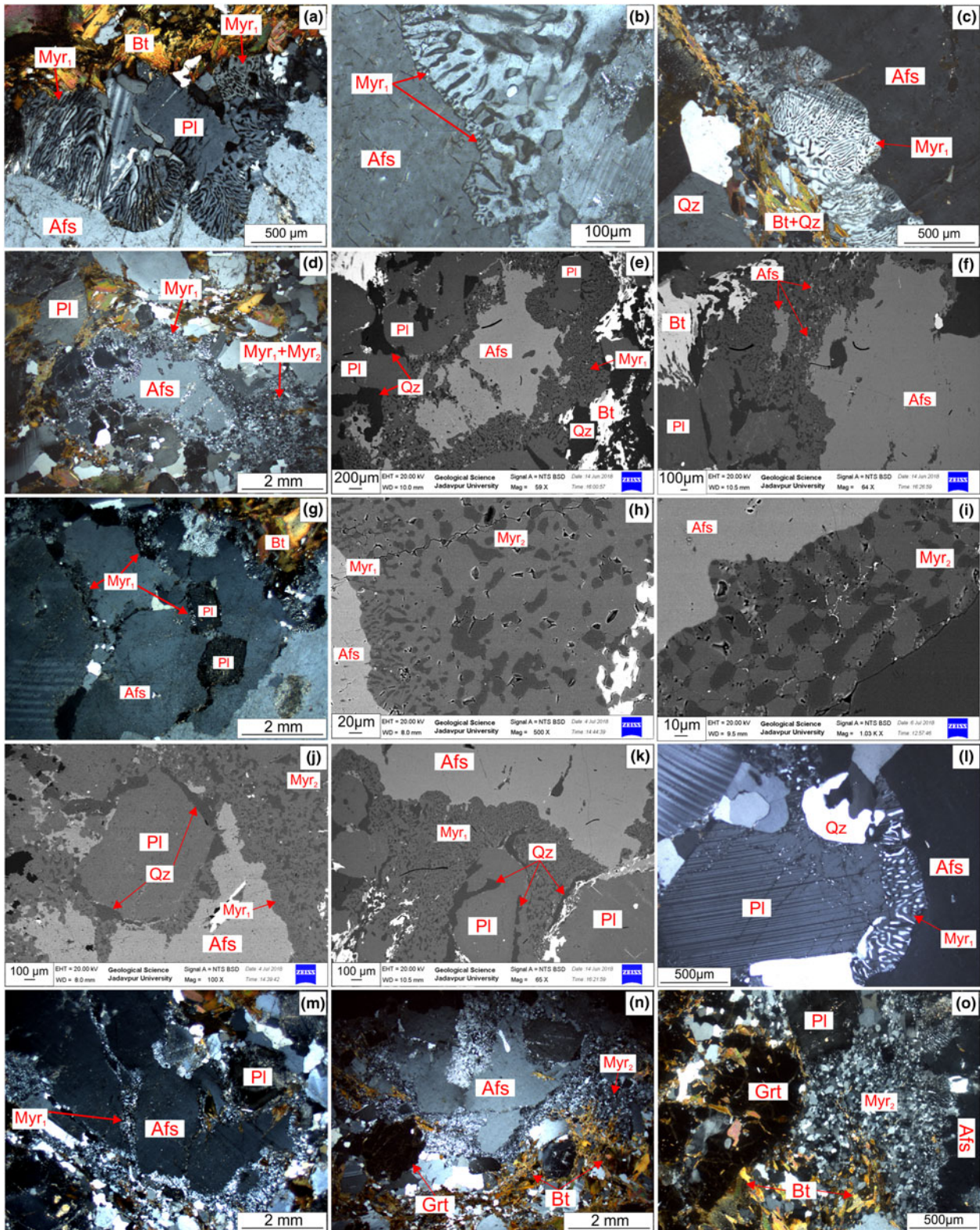
Figure 4. Optical and BSE petrographic characteristics of the quartz–plagioclase myrmekite intergrowths. Mineral abbreviations are after Whitney and Evans (2010). (a–c) Characteristics of Myr1 domains and microtextures of quartz vermiculae. The myrmekite front is bulbous and convex towards alkali-feldspar megacrysts. (d,e) Myrmekite develops all along the periphery of the alkali-feldspar. Myrmekite grows on alkali-feldspar and plagioclase porphyroclasts. (f) Rafts of alkali feldspar, with highly irregular grain boundaries, occur in the Myr1. (g) Myr1 developing at the interface of a plagioclase inclusion within alkali feldspar. (h) Myr1 forms near the alkali feldspar whereas the Myr2 in the same myrmekite develop in the rear part in contact with a plagioclase porphyroclast. (i) Direct contact between Myr2 and alkali feldspar. (j,k) A layer of quartz separates the myrmekite from, and is oriented parallel to, the grain boundary of a plagioclase porphyroclast. (l) The twining in plagioclase porphyroclasts can be traced within the plagioclase base of the myrmekite. (m) Myrmekite forms random veins/apophyses within the alkali feldspar. (n,o) Intimate association of myrmekite and secondary biotite. Secondary biotite replaces garnet and plagioclase porphyroclasts and Myr2.

Mineral compositions

A detailed account of mineralogical composition of the meta-granitoid is given in Chakrabarty *et al.* (2023) and in the following sections only the mineral compositions of the myrmekite-rich samples are described.

Feldspar

The alkali-feldspar porphyroclasts are microcline ($Or_{87.3-89.4}$ $Ab_{10.5-12.9}An_{<1}Cs_{1.3-1.8}$) (Fig. 5a,b; Supplementary table 1a). The symbol 'Or' represents the $KAlSi_3O_8$ molecule, with no reference to Al–Si ordering. The presence of a significant albite component in alkali feldspar suggests that very fine perthitic lamellae might be present. The composition of the recrystallised alkali feldspar is poorer in the albite molecule $Or_{89-92}Ab_{7.8-10.7}$ $An_{<1}Cs_{1.5-1.9}$ (Supplementary table 1a). Small patches of alkali feldspar in the myrmekite are distinctly rich in BaO (1.36–1.75 wt.%) relative to the alkali-feldspar porphyroclasts (0.70–1.08 wt.%, Supplementary table 1a). The composition of these fine-grained remnants of alkali feldspar within Myr1 are $Or_{89.1-92.4}$ $Ab_{7.5-10.4}An_{<1}Cs_{2.5-3.2}$. No significant compositional zoning in the alkali feldspar has been noted close to the myrmekite (Fig. 5b; Supplementary table 1a; Core: $Or_{89.4}Ab_{10.5}An_{<1}Cs_{1.3}$ and Rim immediate to Myr1: $Or_{87.5}Ab_{12.4}An_{<1}Cs_{1.7}$).

The oscillatory zoned plagioclase, presumably inherited magmatic characters, show alternation of relatively anorthite poor ($Ab_{59-61}An_{38-41}Or_{<1}$) and anorthite rich ($Ab_{47-50}An_{49-52}Or_{<1}$) compositions (Supplementary table 1b). Proximal to secondary biotite and myrmekite, the plagioclase porphyroclasts have normal compositional zoning with an anorthite-rich core ($Ab_{50}An_{49}Or_1$) and an anorthite poor rim ($Ab_{57}An_{42.5}Or_{0.5}$, Supplementary table 1b). The plagioclase base of myrmekite has systematic zoning which is presented in the compositional profile in Fig. 5b,c. Plagioclase in Myr1 from the fine-grained variety in contact with alkali feldspar to relatively thick vermicular quartz away from the myrmekite front has a very small decrease in the albite component ($Ab_{61.6}An_{37.9}Or_{0.5-0.9}$ to $Ab_{60.6}An_{38.9}Or_{0.5}$) (Supplementary table 1b). A distinct compositional change is noted between Myr1 and Myr2 where polygonal plagioclase in Myr2 is distinctly anorthite rich ($Ab_{58}An_{41}Or_1$ to $Ab_{53}An_{46}Or_1$; Fig. 5b,c; Supplementary table 1b).

Garnet, biotite and ilmenite

The garnet is almandine-rich with significant spessartine and grossular [$Alm_{77-79}Prp_{8-9}Grs_{7-10}Sps_{5-7}$ with X_{Mg} [$Mg/(Fe^{+2}+Mg)$] = 0.09–0.11] (Supplementary table 1c). Compositional zoning has not been recorded in individual grains. The biotite is Fe-rich and regardless of paragene has X_{Mg} = 0.31–0.33 (Supplementary table 1c). Titanium contents of the biotite vary from 0.24 to 0.27 atoms per formula unit (apfu). The ilmenite has near end-member composition with a small amount of Fe^{3+} (0.03 apfu, Supplementary table 1c).

Physical conditions of myrmekite formation

The sample investigated (c.1.75 Ga emplacement age) shared tectonothermal events at c. 0.95 Ga with the younger felsic
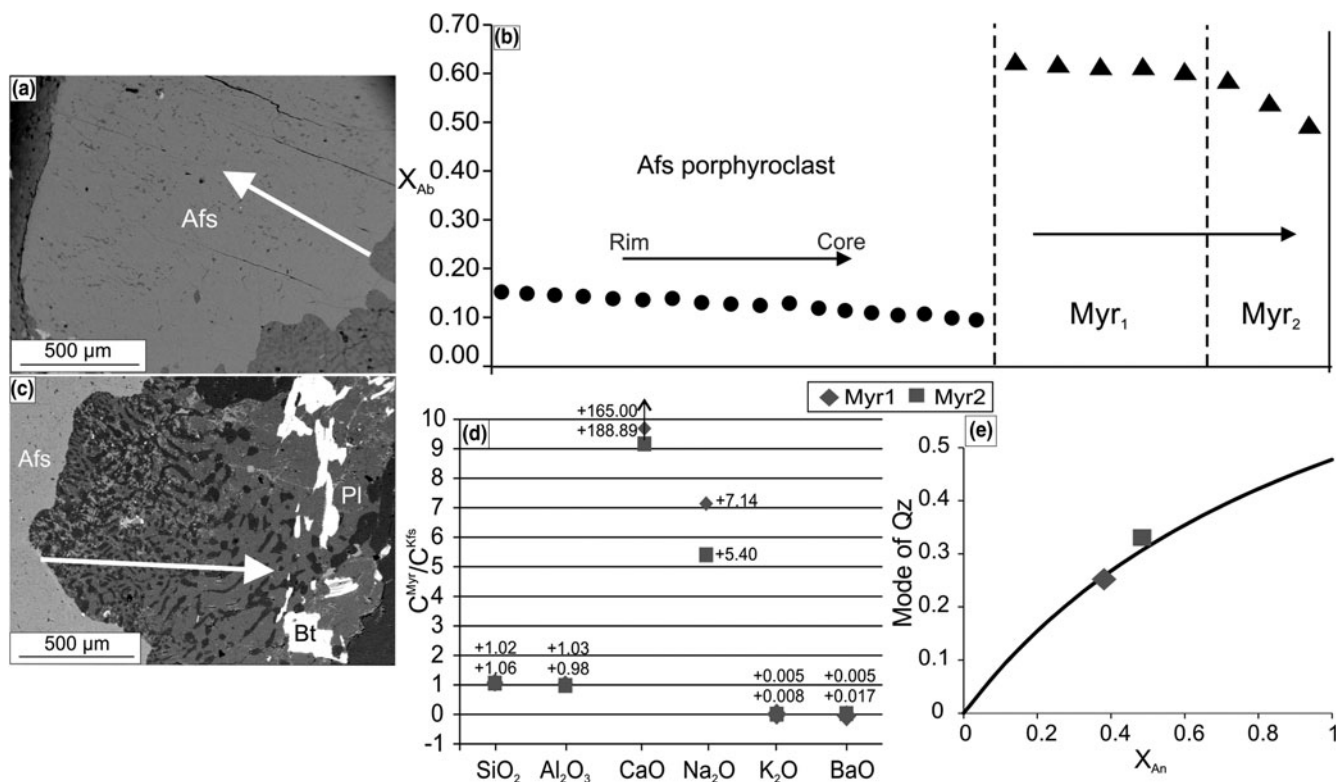

Figure 5. (a) BSE image of the analysed alkali-feldspar porphyroclast. The white arrow represents the direction of the compositional profile from rim to core of the porphyroclast. (b) Compositional profile of alkali-feldspar porphyroclast and plagioclase base of the myrmekite. Black arrows correspond with the white arrows of the BSE images. The composition of alkali feldspar (X_{Ab}) is homogeneous and the plagioclase base in myrmekite has composition zoning. (c) BSE image of the analysed plagioclase base of myrmekite. (d) Change in concentration of mobile and immobile species, involved in myrmekitisation (C'_x/C^o_x where C^o_x and C'_x represent the concentration of a given species x in alkali feldspar and myrmekite), calculated for both Myr1 and Myr2. (e) The curvilinear relation between m_{qtz} and X_{An} as defined by the equation of Abart *et al.* (2014). The modal volumes of quartz, estimated from the BSE images, are plotted against the measured compositions of the corresponding matrix plagioclase in Myr1 and Myr2.

intrusive, now partially retrogressed charnockite with emplacement age of c. 1.4 Ga (Chakrabarty et al., 2022, 2023). Chakrabarty et al. (2022) demonstrated that at the termination of the 0.95 Ga tectonothermal event the rocks of the area studied underwent cooling at nearly constant pressure with extensive hydration in the range of ~500–600°C and ~4–5 kbar. It is, therefore, possible that the secondary biotite and the adjoining myrmekite equilibrated under similar physical conditions. The absence of compositional zoning in alkali feldspars at the immediate contact with the myrmekite suggests that the myrmekitic plagioclase is not in equilibrium with the alkali feldspar. Garnet–biotite thermometry cannot be used for this sample as the garnet and secondary biotite are not in equilibrium. Regardless, recrystallisation of alkali feldspar requires temperatures $\geq 500°C$ (Vernon, 2004; Harlow and Wirth, 2000; Menegon et al., 2006). A temperature greater than 500°C is considered to be favourable for myrmekite formation, with oligoclase and more calcic plagioclase (Harlow and Wirth, 2000). Pressures below 5.5 kbar at $\geq 500°C$ are consistent with the absence of epidote/clinozoisite. In summary, these data confirm the proposition that myrmekite and the secondary biotite were formed during the terminal phase of the 0.95 Ga tectonothermal event (500°–600°C and 4–5 kbar).

Controls of mobile and immobile species during the formation of myrmekite

Mass-balance approach

The composition of the alkali feldspar is grossly different from the composition of the myrmekite intergrowth replacing alkali feldspar. This implies that a number of components should be mobile during the myrmekitisation of the alkali feldspar (e.g. Simpson and Wintsch, 1989; Vernon 1991, 2004; Cisneros-Lazaro et al., 2019; Abart et al., 2012, 2014). Fluid mediated, interface-controlled, solution–reprecipitation processes (Putnis, 2002) are consistent with a number of textural features presented in this study including: (a) the bulbous outlines of the myrmekite that are convex towards the precursor alkali feldspar; and (b) the presence of relict patches of alkali feldspar within the myrmekite. The intimate association of myrmekite with the secondary biotite replacing garnet and plagioclase porphyroclasts with albitic rims, suggests a genetic connection between the two processes. The nature and extent of element mobility (or immobility) across the myrmekite–alkali-feldspar boundary will be assessed initially and followed by evaluation of the genetic connection between the myrmekite formation on the alkali feldspar and the hydration of the garnet and plagioclase in the immediate vicinity.

Element mobility (immobility) during the myrmekite formation: behaviour of Al and Si

Quantification of the extent of element mobility across the myrmekite–alkali-feldspar boundary requires a reference frame. The concentration of at least one immobile element can serve as a good reference frame against which enrichment/depletion of mobile elements can be quantified (Ague, 2003; Philpotts and Ague, 2009). A number of studies have documented that Al and Si remain essentially immobile during the myrmekitisation of alkali feldspar (Cisneros-Lazaro et al., 2019; Abart et al., 2014; Cesare et al., 2002). However, studies have demonstrated that Al and Si can be mobile on different length scales during a metasomatic process (reviewed in Roy Choudhury et al., 2023; Chatterjee et al., 2022). The behaviour of Al (and Si) should be

evaluated in each individual case before using Al as a reference frame for quantification of the extent of mobile elements.

In this work we have adopted two approaches to understand the behaviour of Al and Si during the formation of myrmekite after alkali feldspar.

Approach 1. It has been demonstrated in a number of studies (reviewed in Philpotts and Ague, 2009) that any immobile element during metasomatism should follow the relation:

$$C_i^o M_i^o = C_i' M_i' \tag{1}$$

Where C_i^o and C_i' represent the concentrations (in ppm, wt%) of any immobile species 'i' and M_i^o and M_i' are the masses of precursor and altered rocks, respectively.

Equation 1 leads to the relationship that all the immobile elements will have same C_i'/C_i^o ratio in a given metasomatic environment. For a given set of C_i' and C_i^o, the amount of enrichment and depletion of the mobile elements can be quantified by the relation (cf. Philpotts and Ague, 2009):

$$\Delta n_j\% = [(C_i^o/C_i') \times (C_j'/C_j^o) - 1]\% \tag{2}$$

C_j^o and C_j' are the concentration of the mobile species 'j' in the precursor and metasomatic rocks. Δn_j is the % change of the species j (negative and positive signs of Δn_j indicate depletion and enrichment of the species j in the metasomatic zone, respectively).

In this study, the phase composition of alkali feldspar and the bulk composition of the myrmekite are considered as the M_i^o and M_i' for the alkali-feldspar–myrmekite system. Leaving out trace elements, the composition of myrmekite–alkali feldspar can be represented in the six component system (K_2O–Na_2O–BaO–CaO–Al_2O_3–SiO_2). The bulk composition of the myrmekite has been computed combining the volume proportion of the quartz and plagioclase from the BSE image and their measured compositions ('microbulk'; Stuwe 1997, Evans 2004). Supplementary table 1d and Fig. 5d represent the C_x'/C_x^o (C_x^o and C_x' represent the concentration of a given species x in alkali feldspar and myrmekite). The ratios C_{Al2O3}'/C_{Al2O3}^o and C_{SiO2}'/C_{SiO2}^o in the alkali feldspar–myrmekite pair match perfectly within the uncertainties of measurement of mineral composition and 'microbulk' composition of myrmekite (both Myr1 and Myr2, Supplementary table 1d and Fig. 5d). The match between the two parameters is the best for the alkali feldspar–Myr1 pair. This observation supports the view that SiO_2 and Al_2O_3 remained essentially constant during the formation of myrmekite after alkali feldspar. The ratios of C_x'/C_x^o for CaO, Na_2O, K_2O and BaO deviates significantly from C_{Al2O3}'/C_{Al2O3}^o (or C_{SiO2}'/C_{SiO2}^o, Supplementary table 1d, Fig. 5d) and are, therefore, considered as mobile components during the myrmekite formation after alkali feldspar (Philpotts and Ague, 2009).

Approach 2. For Al and Si being conserved, the modal volume of quartz in the myrmekite follows a curvilinear relationship with the anorthite content (X_{An}) of the matrix plagioclase (Ashworth, 1972, Abart et al., 2014). This relation is expressed by the equation (Abart et al., 2014):

$$m_{qtz} = 4X_{An} \times V_{qtz}/(4X_{An} \times V_{qtz} + V_{plg}) \tag{3}$$

m_{qtz}, V_{qtz} and V_{plg} are the modal quartz, volume of quartz and volume of plagioclase, respectively.

In Fig. 5e the curvilinear relation between m_{qtz} and X_{An} as defined by equation 3 is shown. The V_{qtz} and V_{plg} are calculated

at 550°C and 5 kbar pressure, the probable physical condition of myrmekite formation in the sample investigated.

The modal volumes of quartz, estimated from the BSE images, are plotted against the measured compositions of the corresponding matrix plagioclase in Myr1 and Myr2 (Fig. 5e). Both Myr1 and Myr2 are plotted close to the theoretical line (equation 3) for their corresponding X_{An}. The close correspondence of the theoretical and observed modal quartz for a given X_{An} of plagioclase corroborate the observation of Approach 1 that Al and Si were effectively conserved during the myrmekite formation after alkali feldspar. Similar to Approach 1, improved correspondence between theoretical and observed modal quartz values at a given X_{An} was noted for Myr1.

Using Al as a reference frame, application of equation 2 shows a very large loss of K_2O (Myr1 = 100%, Myr2 = 99%) and BaO (Myr1 = 100% and Myr2 = 98%) and gain in Na_2O (Myr1 = 614% and Myr2 = 440%) and CaO (Myr1 = 16400% and Myr2 = 18,789%) during the formation of myrmekite after alkali feldspar (Supplementary table 1d).

For conserved Si and Al, the balanced metasomatic reaction that presumably operated across the myrmekite–alkali-feldspar interface can be modelled. The measured compositions of alkali feldspar and plagioclase matrix of myrmekite (quartz is considered as pure SiO_2) are used as input parameters. Details of the textural modelling study with C-Space are discussed in a number of publications (Roy Choudhury et al., 2023). With respect to the variation in the compositions of matrix plagioclase, the balanced reactions are obtained for Myr1 and Myr2 separately, and are shown in Table 1 as equations 4 and 5.

The ΔV_S represents the volume change of the solid phases (product − reactant phases) expressed in percentages. A negative value of ΔV_S suggests negative volume change of 9.5–10% during the formation across the myrmekite–alkali-feldspar interface. The estimated volume reduction during the formation of myrmekite in this work compares well with the volume reduction of −10% reported by Simpson and Wintsch (1989), during myrmekite formation. The modal ratios of quartz and matrix plagioclase calculated from the balanced reactions 4 and 5 (expressed as $V_{Pl}:V_{Qz}$) matches well with the observed ratio of quartz and plagioclase in Myr1 (calculated = 1:3, observed = 1:3) and Myr2 (calculated = 1:2.2, observed = 1:2). The balanced chemical reactions (4, 5) are consistent with the results of the mass-balance calculation and suggest addition of Ca and Na, and removal of K during replacement of alkali feldspar by myrmekite.

Element mobility during the formation of the secondary biotite

Textural features suggest an intimate relationship between myrmekite (both Myr1 and Myr2), secondary biotite that replaces plagioclase and garnet porphyroclasts. Textural modelling was done with the C-Space program using the measured compositions of secondary biotite, compositions of garnet and plagioclase porphyroclasts (calcic core and albitic rim as separate entities) as input parameters. The textural modelling returns the mass-balanced metasomatic reactions given in Table 2, equation 6.
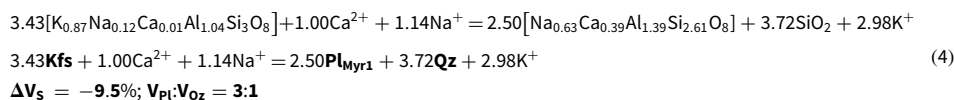
The modelled reaction explains the replacement of secondary biotite after garnet and plagioclase porphyroclasts and normal zoning in the latter phase at the contact of secondary biotite. The release of Ca^{2+} and consumption of K^+ as seen in the modelled reaction 6 are likely to facilitate the growth of myrmekite in the adjoining alkali feldspar. Reactions 4-6 requires addition of Na^+ to progress to the right. Hence, though local redistribution of Ca^{2+} and K^+ could explain the feedback mechanism between formation of myrmekite and secondary biotite, Na^+ has to be transported further as the secondary biotite and albitic rims on plagioclase porphyroclasts develop throughout the rock irrespective of the occurrence of the alkali feldspar and myrmekite.

Thermodynamic drive on the formation of myrmekite and secondary biotite: the chemical potential diagram

The balanced chemical reactions (equation 4–6) obtained from the textural modelling study suggest that Ca, Na and K behaved as mobile elements during formation of secondary biotite. Reactions 4–6 also suggest that behaviour of Ca and K are opposite in myrmekite- and biotite-forming reactions. Both the reactions, however, consume Na in variable proportions. In addition, H_2O was consumed in reaction 6. It is well known that chemical mass transfer is controlled primarily by chemical potential differences of the transporting chemical species (e.g. Ca, Na and K, reviewed in Philpotts and Ague, 2009). In order to demonstrate the directions of the chemical gradients of the mobile species during the formation of myrmekite and secondary biotite, isothermal–isobaric μ_{CaO}–μ_{K2O} diagrams are constructed at different pressure/temperature conditions (Fig. 6). The system K_2O–CaO–FeO–Al_2O_3–SiO_2–H_2O (KCFASH) has been chosen with garnet, biotite, chlorite, muscovite, plagioclase, K-feldspar and quartz. In view of the pervasive occurrence of biotite in the rock studied, H_2O has been considered as an excess phase. Three invariant points are considered. These are: (1) [muscovite, K-feldspar]; (2) [chlorite, K-feldspar]; and (3) a degenerate invariant point [garnet, biotite, chlorite]. A temperature of 550°C and pressure of 5 kbar, the probable P–T condition of formation of myrmekite and secondary biotite (discussed early), are used to calculate the μ_{CaO}–μ_{K2O} diagram in the system KCFASH (Fig. 6). To account for the Na_2O and MgO, the activities of phases of the μ_{CaO}–μ_{K2O} diagrams are calculated from the measured

---

Table 1. Myrmekite reactions used in the text.

The balanced chemical reaction for Myr1:

$$3.43[K_{0.87}Na_{0.12}Ca_{0.01}Al_{1.04}Si_3O_8] + 1.00Ca^{2+} + 1.14Na^+ = 2.50[Na_{0.63}Ca_{0.39}Al_{1.39}Si_{2.61}O_8] + 3.72SiO_2 + 2.98K^+$$

$$3.43\textbf{Kfs} + 1.00Ca^{2+} + 1.14Na^+ = 2.50\textbf{Pl}_{Myr1} + 3.72\textbf{Qz} + 2.98K^+ \quad (4)$$

$$\Delta V_S = -9.5\%; \; V_{Pl}:V_{Qz} = 3:1$$

The balanced chemical reaction for Myr2:

$$4.06[K_{0.87}Na_{0.12}Ca_{0.01}Al_{1.04}Si_3O_8] + 1.38Ca^{2+} + 1.00Na^+ = 2.81[Na_{0.54}Ca_{0.47}Al_{1.49}Si_{2.51}O_8] + 5.04SiO_2 + 3.51K^+$$

$$4.06\textbf{Kfs} + 1.38Ca^{2+} + 1.00Na^+ = 2.81\textbf{Pl}_{Myr2} + 5.04\textbf{Qz} + 3.51K^+ \quad (5)$$

$$\Delta V_S = -10\%; \; V_{Pl}:V_{Qz} = 2.2:1$$
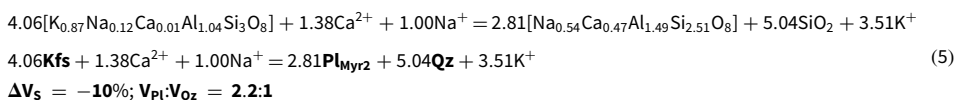
Table 2. Mass-balanced metasomatic reaction.

$15.30\{(Fe_{2.45}Mg_{0.27}Ca_{0.22})Al_{1.98}Si_3O_{12}\} + 20.57SiO_2 + 1.00Na^+ + 19.78K^+ + 19.94H_2O =$

$\quad 19.60\{K_{0.92}(Fe_{1.75}Mg_{0.79})Al_{1.41}Si_{2.68}O_{10}(OH)_2\} + 1.64\{Na_{0.58}Ca_{0.43}Al_{1.41}Si_{2.58}O_8\} + 3.20Ca^{2+}$

$15.30\mathbf{Grt} + 20.57\mathbf{Qz} + 1.00Na^+ + 19.78K^+ + 19.94H_2O = 19.60\mathbf{Bt} + 1.64\mathbf{Pl_{Rim}} + 3.20Ca^{2+}$

$\Delta V_S = \mathbf{+46.5}\%$

(6)
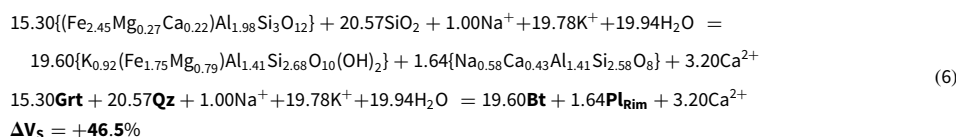
compositions of the solid-solution phases. The activity adjusted chemical potential diagram is shown. Considering the two distinct compositions of the myrmekites the chemical potential diagrams are calculated for two plagioclase compositions (Myr1 and Myr2) (Fig. 6a). In the absence of chlorite, the activity of chlorite is set as unity (Fig. 6a,c,d). However the topology of the chemical potential diagrams do not change significantly other than the invariant points coming closer in the chemical potential diagram (Fig. 6b). To demonstrate the effects of pressure and temperature on the topology, a specific plagioclase composition (Myr1) at 550°C and 5 kbar are chosen for reference (Fig. 6c,d).

The following observations can be made from the different μ_{CaO}–μ_{K2O} diagrams: The isothermal–isobaric univariant reaction that connects I_1 and I_2, explains the formation of secondary biotite after garnet and has lower μ_{K2O} than the myrmekite-forming reaction that emanates from I_3 (Fig. 6). Similarly, the reaction at the sites of secondary biotite and the myrmekite front creates a gradient of μ_{CaO} towards the latter (Fig. 6a). Pressure / temperature being constant, Myr2 with more calcic plagioclase forms at lower μ_{K2O} and μ_{CaO} than the Myr1 (less calcic, Fig. 6a). Pressure and temperature have a significant effect on the phase relationship on myrmekite stability. Other factors being constant, higher pressure and lower temperature expand the stability field of plagioclase + quartz (relative to alkali feldspar) and promote myrmekite formation (Fig. 6c,d). The opposite scenario, heating and decompression impede the growth of myrmekite unless the composition of the fluid overpowers the effect of these parameters.

Discussion

The analytical data provide clues regarding the control of pressure, temperature, deformation and metamorphic/metasomatic fluid on the formation of myrmekite in the meta-porphyritic rocks investigated. In the following section the roles of various parameters are evaluated on the basis of data presented above.

Role of deformation and physical conditions on myrmekite growth

Petrographic studies suggest two stages of myrmekite formation which resemble the myrmekite described from Pofadder shear zone, Namibia (Cisneros-Lazaro *et al.*, 2019). However, unlike this and many other studies (e.g. Simpson and Wintsch, 1989; Vernon 1991; Menegon *et al.*, 2006), the microstructural features of the rock studied here do not support myrmekite formation in a shear zone, although evidence of deformation of various intensities are observed in field and petrographic studies. The polygonal aggregates of Myr2 that presumably formed early, clearly indicate strain-induced recrystallisation that minimised the interfacial energy among the grains (Vernon 2004; Cisneros-Lazaro *et al.*, 2019). Microtextural information remains inconclusive

regarding the origin of the coarse, locally polygonal, aggregates of Myr2. There exist two possibilities as argued by Cisneros-Lazaro *et al.* (2019). One possibility is that the Myr2 initially had a vermicular morphology and subsequent recrystallisation and grain growth at high temperature led to the larger aggregates with planar-to-gently curved grain contacts (relative to Myr1). The other option is that coarser grains in Myr2 did not occur from a vermicular intergrowth and formed directly from alkali feldspar at high temperature and fluid pressure. Both these factors contributed to large length of transport of chemical species so that the product grains have planar contacts with minimum surface energy (Philpotts and Ague, 2009). Regardless of these two options, the role of deformation on the formation of Myr2 seems to be well-founded in the sample investigated. Unlike Myr2, control of stress on the formation of Myr1 is not straightforward. The growth of vermicular myrmekite on alkali feldspar is the subject of debate. Asymmetric concentration of vermicular myrmekite on the surface of alkali-feldspar porphyroclasts that are at a high angle to the direction of compression led Simpson and Wintsch (1989) to conclude that a high concentration of tangled dislocation/elastic strain energy on the alkali-feldspar surface promoted the growth of myrmekite. In contrast, Vernon (1991) argued that stress is a required, but not essential condition for the growth of vermicular myrmekite on alkali feldspar. An ambient stress regime, in most cases, only facilitated the access of fluid that triggered the replacement of alkali feldspar by a vermicular intergrowth of plagioclase and quartz. Corroborating other studies (Simpson and Wintsch, 1989), the stoichiometrically balanced reaction (reaction 4) in this study suggests ~10% shrinkage in solid volume during formation of the two generations of myrmekite. It then follows that pressure increase or temperature decrease, facilitates the myrmekite-forming reaction. Studies have shown that myrmekite begins to form at the interface of plagioclase and alkali feldspar, and moves into the alkali feldspar as the process continues. Thus, a decrease in temperature is consistent with smaller thickness and interlamellar spaces between quartz vermiculae at the frontal part of the myrmekite interface and progressively thicker and more widely spaced quartz vermiculae in the distal part of Myr1 (Harlov and Writh 2000; Abart *et al.*, 2014). The regional P–T path and the estimated temperature corroborate the growth of myrmekite during a phase of cooling at 500–600°C and 4–5 kbar pressure. As a drop in pressure increases the rock volume, it is unlikely that myrmekite formation, which in this area requires an ~10% volume change, was formed during a steeply decompressive P–T path. Indeed, tangled dislocations/elastic-strain energy concentrate on the surface that is at high angles to the direction of shortening. The accrued elastic energy on the surface increases the Gibbs Free energy (or chemical potential) locally, thereby making the surface of high strain energy of alkali feldspar prone to replacement by myrmekite (discussed in Vernon, 2004; Philpotts and Ague, 2009).
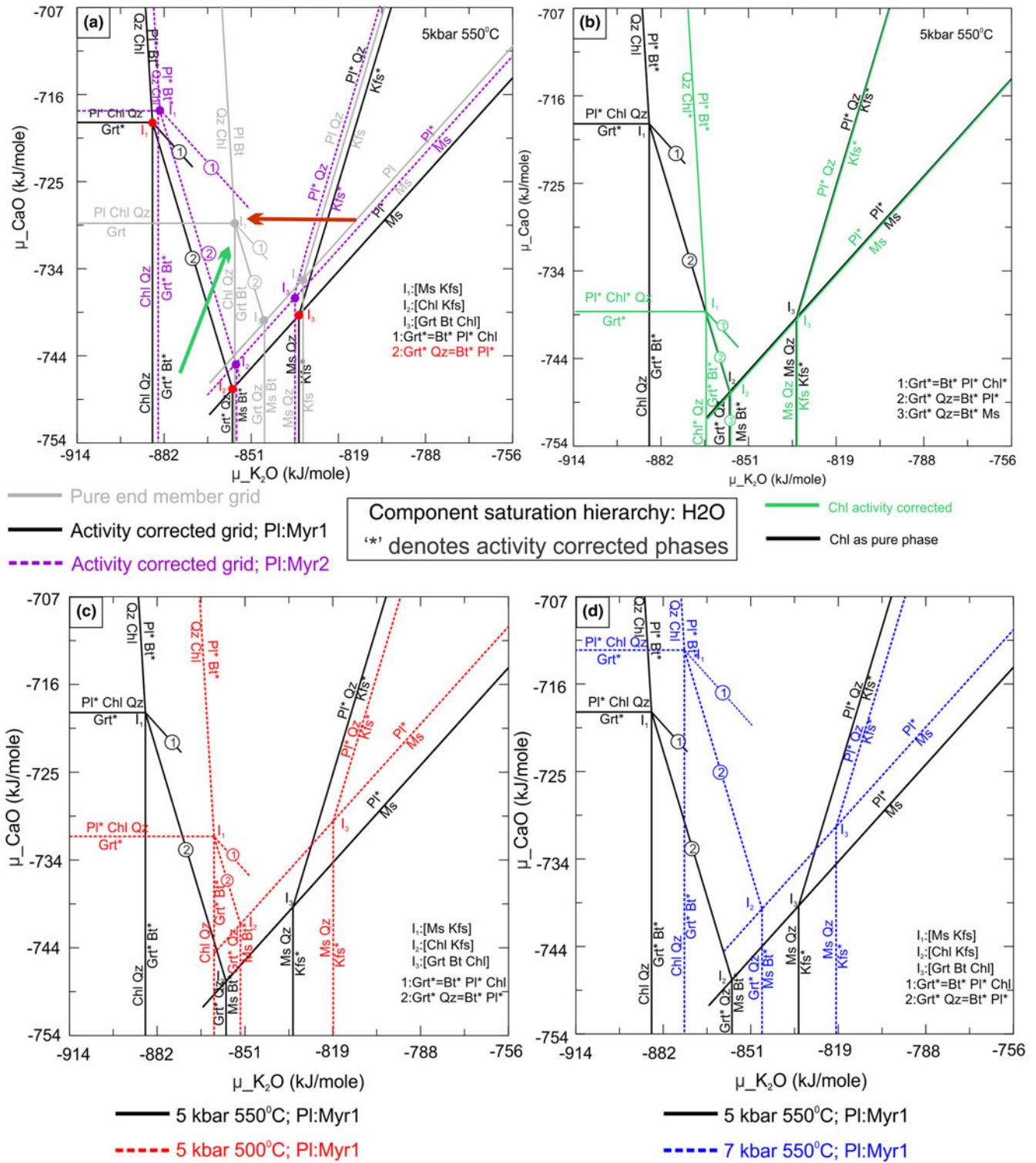
Figure 6. The μ_{CaO}–μ_{K2O} diagrams in the system KCFASH. (a) Isothermal–isobaric (iT-iP) chemical potential (μ) diagrams have been computed in NCKFASH system at 550°C and 5 kbar. The grey coloured grid represents the reactions and invariant points calculated with pure end-members of the minerals. The black grid represents reactions with activity corrected compositions of minerals (except chlorite, muscovite) and plagioclase with the composition of Myr1. The purple grid denotes reactions with a plagioclase composition of Myr2. (b) The topology of the chemical potential diagrams does not change significantly other than the invariant points coming closer to each other for chlorite pure and activity corrected compositions. (c,d) Effects of pressure and temperature on μ_{CaO} vs μ_{K2O} for a specific plagioclase composition (Myr1).

A number of features in the rocks investigated suggest minimal contribution of stress, if any, during the growth of Myr1. Thus, the pervasive development of Myr1 along the periphery of the alkali feldspar, in both megacrystic and matrix grains, and at the interface of plagioclase inclusions in alkali feldspar suggests that growth of Myr1 was likely to be unrelated to local kinematic

axes (Cesare *et al.*, 2002; Menegon *et al.*, 2006). The delicate intergrowth of quartz and plagioclase in Myr1 are not expected to sustain high deviatoric stress (Vernon, 1991). The intimate association of Myr1 and secondary biotite indicate static growth.

The optical continuity of plagioclase porphyroclasts and the base plagioclase of Myr 1 suggest heterogeneous nucleation and consequent epitaxial growth of the latter on the former (Vernon, 1991). This feature is inconsistent with the preferential growth of Myr1 on the high-strain surface of alkali feldspar. Considering all the evidence, it seems reasonable to conclude that deformation did not have a major control on the formation of Myr1.

Role of fluid in the formation of myrmekite

Several textural features including a highly irregular myrmekite front, and preservation of small rafts of alkali feldspar within the myrmekite suggest that myrmekite in these rocks formed by replacement of alkali feldspar (Becke, 1908; Phillips, 1974; Simpson and Wintsch, 1989; Vernon 2004; Abart *et al.*, 2014; Menegon *et al.*, 2006; Ceccato *et al.*, 2018; Cisneros-Lazaro *et al.*, 2019). Together with the original work of Becke (1908) and the references cited above, the balanced chemical reactions (reaction 4, 5) derived in this work provide additional support for the replacement theory. Replacement of alkali feldspar by myrmekite is a metasomatic process in the sense that composition of the precursor alkali feldspar is grossly different from the product myrmekite that replaces it. Subsequent to Becke (1908), several studies, and this present work, argue that to accomplish 'myrmekitisation', Ca and Na need to be added to, and K (and Ba) be removed from, the alkali feldspar (Collins, 2013), whereas Al and Si remain immobile during the myrmekite formation. Deformation might have a role in determining the site of nucleation and the morphology of the myrmekite as in the case of Myr2. However, mass transport along the chemical potential gradients of the chemical species (Ca and Na towards and K away from the myrmekite front) is a prerequisite condition for chemical transformation of alkali feldspar to myrmekite (cf. Philpotts and Ague, 2009). Owing to slow kinetics, purely thermally driven grain-boundary diffusion of Ca, Na and K with no fluid mediation cannot explain the extensive growth of myrmekite to the lengths observed in our work (e.g. Philpotts and Ague, 2009). A fluid-mediated transport of Ca+ Na and K (in the reverse direction) seems to be the triggering force for formation of myrmekite (Becke, 1908; Simpson and Wintsch, 1989; Vernon, 1991; Cisneros-Lazaro *et al.*, 2019). The intimate association of secondary biotite and myrmekite further corroborate the fluid-mediated material transport during the formation of myrmekite. Similar fluid-induced metasomatic changes have also been reported from Jalore and Siwana granites of India, where K-feldspar porphyroclasts are mantled by plagioclase (Mondal *et al.*, 2017). These authors infer that the presence of well-defined and corroded boundaries between the mantle and the core, protrusion of apophyses into the megacryst interiors, stranded inclusions of K-feldspar within the oligoclase mantle and preservation of the original megacrystic grain boundaries advocates for pseudomorphic replacement through coupled dissolution–reprecipitation replacement processes.

The textural features that support the intimate association of myrmekite and secondary biotite can be explained from the isothermal–isobaric μ_{CaO}–μ_{K2O} diagrams. The topology of these chemical potential diagrams (Fig. 6) suggests that fluid that is

in equilibrium with the myrmekite has higher μ_{K2O} than the fluid in equilibrium with the biotite-forming reaction, a sink of K_2O (Fig. 6a–d). Consequently, K_2O that is generated at the myrmekite front will move towards garnet and plagioclase porphyroclasts along its chemical potential gradient and trigger the growth of biotite (reaction 4, 5, 6 brown arrow in Fig. 6a). The process, in turn, releases CaO and hence increases μ_{CaO} of the fluid at this end (green arrow in Fig. 6a). Myrmekite formation consumes CaO and hence, creates a local low μ_{CaO} environment. This allows CaO to move from secondary biotite domain to myrmekite front. This coupled mass transfer, marked by reactions 4, 5, 6 continues until: (1) sufficient fluids that could dissolve and transport K_2O and CaO (also Na_2O) are available; and (2) the fluid gains access to the reactant phases of secondary biotite- and myrmekite-forming reactions. Because grain contacts act as fluid conduits (Putnis and Austrheim, 2010), pervasive development of myrmekite and secondary biotite all along the grain contacts can be linked to pervasive fluid flow as reviewed by Dempster *et al.* (2021), Menegon *et al.* (2006) and Cesare *et al.* (2002).

From this observation it does not follow that the formation of pervasive secondary biotite in the entire volume of the rock studied are produced by local reorganisation of various elements. Rather, pervasive infiltration driving the processes that formed secondary biotite together with the accompanying albite rim on plagioclase porphyroclasts, also possibly triggered the growth of myrmekite after alkali feldspar. This observation is corroborated by the inference of Chakrabarty *et al.* (2022), who demonstrated that all the rocks of the Makrohar Granulite Belt (Fig. 1b, c) were extensively retrogressed during the terminal phase of the c. 0.95 Ga tectonothermal event. In a recent publication, Touret *et al.* (2022) argued that myrmekite on alkali feldspar marks the pathways along which mantle-derived brines traversed the rocks. The low dihedral angle that the brine molecules make with silicate minerals allows the brines to move rapidly and pervasively through the rock (Touret *et al.*, 2022, Plümper and Putnis, 2009). Albitisation of plagioclase and K-metasomatism are considered to be common phenomena in brine-induced metasomatic rocks (Plümper and Putnis, 2009). Pervasive development of secondary biotite and the accompanying albite-rich rim on plagioclase porphyroclasts and myrmekite seem to support the postulation of Touret *et al.* (2022).

A volume reduction of ~10% during myrmekite formation created 'reaction enhanced secondary porosity' that facilitated fluid movement towards alkali feldspar and triggered the growth of myrmekite (Putnis and Austrheim, 2010). However, a large positive volume change (~46.5%) of the secondary biotite-forming reaction (reaction 6) is expected to create a fluid overpressure and lead to microfractures along which the fluid could move (reviewed in Dempster *et al.*, 2021). Regional deformation also provided access to the infiltrating fluid that is consistent with the formation of biotite foliation with one mode of secondary biotite being syntectonic with the regional deformation. Development of secondary biotite and Myr1 on all the sides of plagioclase porphyroclasts and alkali feldspar, respectively, suggest a feedback mechanism driven by pervasive fluid flow.

Conclusion

From our investigations of a myrmekite-bearing meta-porphyritic granitoid in the northern part of the Central Indian Tectonic Zone we conclude the following:

(1) Myrmekite develops and replaces alkali-feldspar megacrysts along all their peripheries. Myrmekite nucleates on plagioclase porphyroclasts and the myrmekite front moves into the alkali feldspar. Myrmekite and secondary biotite form together.

(2) Deformation had a significant contribution in forming the polygonal aggregates of Myr2, although field and microtextural features do not support any control of deformation during the formation of Myr1. The cooling of the complex is responsible for the variation in quartz morphology found in myrmekite.

(3) Reaction modelling and the mass-balance calculations suggest that Ca and Na are added to, and K is removed from, the alkali feldspar during the myrmekite formation at essentially constant Si and Al. The secondary biotite-forming reaction, however, consumes K and releases Ca.

(4) Different isothermal–isobaric sections of μK_2O–μCaO in the KCFASH system suggest that CaO and K_2O moved in the opposite direction during myrmekitisation and along their respective chemical potential gradients that are created between the reaction sites.

(5) The feedback mechanism that operated between the two reaction sites were controlled by infiltration of brine-rich fluid in the meta-granitoid during a regional hydration event (550–$600^{o}C$ and 5–6 kbar).

Supplementary material. The supplementary material for this article can be found at https://doi.org/10.1180/mgm.2023.90.

Competing interests. The authors declare none.

References

Abart R., Heuser D. and Habler G. (2014) Mechanisms of myrmekite formation: case study from the Weinsberg granite, Moldanubian zone, Upper Austria. *Contributions to Mineralogy and Petrology*, **168**, 1074.

Abart R., Petrishcheva E. and Joachim B. (2012) Thermodynamic model for growth of reaction rims with lamellar microstructure. *American Mineralogist*, **97**, 231–240.

Ague J.J. (2003) Fluid infiltration and transport of major, minor, and trace elements during regional metamorphism of carbonate rocks, Wepawaug Schist, Connecticut, USA. *American Journal of Science*, **303**, 753–816, https://doi.org/10.2475/ajs.303.9.753

Ashworth J.R. (1972) Myrmekites of exsolution and replacement origins. *Geological Magazine*, **109**, 45–62.

Ashworth J.R. (1986) Myrmekite replacing albite in prograde metamorphism. *American Mineralogist*, **71**, 895–899.

Becke F. (1908) XV. Mitteilungen der Wiener Mineralogischen Gesellschaft. *Mineralogy and Petrology*, **27**, 377–391.

Bhowmik S.K. (2019) The current status of orogenesis in the Central Indian Tectonic Zone: A view from its Southern Margin. *Geological Journal*, **54**, 2912–2934, https://doi.org/10.1002/gj.3456

Ceccato A., Menegon L., Pennacchioni G. and Morales L.F.G. (2018) Myrmekite and strain weakening in granitoid mylonites. *Solid Earth*, **9**, 1399–1419.

Cesare B., Marchesi C. and Connolly J.A.D. (2002) Growth of myrmekite coronas by contact metamorphism of granitic mylonites in the aureole of Cima di Vila, Eastern Alps, Italy. *Journal of Metamorphic Geology*, **20**, 203–213.

Chakrabarty A., Karmakar S., Mukherjee S. and Roy S. (2022) Neoproterozoic reworking of a Mesoproterozoic magmatic arc from the north-eastern part of the Central Indian Tectonic Zone: Implication for the growth and disintegration of the Indian shield in the Proterozoic supercontinental cycles. *Precambrian Research*, **378**, 106758.

Chakrabarty A., Mukherjee S., Karmakar S., Sanyal S. and Sengupta P. (2023) Petrogenesis and in situ U-Pb zircon dates of a suite of granitoid in the northern part of the Central Indian tectonic zone: Implications for prolonged arc magmatism during the formation of the Columbia supercontinent. *Precambrian Research*, **387**, 106990, https://doi.org/10.1016/j.precamres.2023.106990

Chatterjee S., Karmakar S., Mukherjee S., Sanyal S. and Sengupta S. (2022) Origin of clinopyroxene-ilmenite symplectites in mafic granulites from eastern parts of the Chotanagpur granite gneissic complex, East Indian shield. *American Mineralogist*, **108**, https://doi.org/10.2138/am-2022-8715

Chattopadhyay A., Bhowmik S.K. and Roy A. (2020) Tectonothermal evolution of the Central Indian Tectonic Zone and its implications for Proterozoic supercontinent assembly: The current status. *Episodes*, **43**, 132–144, https://doi.org/10.18814/epiiugs/2020/020008

Chowdhury P., Talukdar M., Sengupta P., Sanyal S. and Mukhopadhyay D. (2013) Controls of P-T path and element mobility on the formation of corundum pseudomorphs in Paleoproterozoic high-pressure anorthosite from Sittampundi, Tamil Nadu, India. *American Mineralogist*, **98**, 1725–1737.

Cisneros-Lazaro D.G., Miller J.A. and Baumgartner L.P. (2019) Role of myrmekite and associated deformation fabrics in controlling development of granitic mylonites in the Pofadder Shear Zone of southern Namibia. *Contributions to Mineralogy and Petrology*, **174**, 1–20. Springer.

Collins L.G. (2013) Origin of myrmekite as it relates to K-, Na-, and Ca-metasomatism and the metasomatic origin of some granite masses where myrmekite occurs. No. 56, electronic documents, http://www.csun.edu/~vcgeo005/index.html

Connolly J.A.D. (2005) Computation of phase equilibria by linear programming: A tool for geodynamic modeling and its application to subduction zone decarbonation. *Earth and Planetary Science Letters*, **236**, 524–541.

Connolly J.A.D. (2009) The geodynamic equation of state: What and how. *Geochemistry, Geophysics, Geosystems*, **10**, https://doi.org/10.1029/2009GC002540

Dempster T.J., Hollinsworth A.D., McIntosh E., Edgar S., Faithfull J.W. and Koehn D. (2021) Deformation-induced and reaction-enhanced permeability in Metabasic Gneisses, Iona, Scotland: controls and scales of retrograde fluid movement. *Geofluids*, **2021**, 1–18.

Evans T.P. (2004) A method for calculating effective bulk composition modification due to crystal fractionation in garnet-bearing schist: Implications for isopleth thermobarometry. *Journal of Metamorphic Geology*, **22**, 547–557. https://doi.org/10.1111/j.1525-1314.2004.00532.x

Fouqué F. and Michel-Lévy A. (1879) *Minéralogie Micrographique, 2 vol.* Memoires et Cartes geologiques de France, 153 pp.

Harlov D.E. and Wirth R. (2000) K-feldspar–quartz and K-feldspar–plagioclase phase boundary interactions in garnet–orthopyroxene gneiss's from the Val Strona di Omegna, Ivrea–Verbano Zone, northern Italy. *Contributions to Mineralogy and Petrology*, **140**, 148–162.

Holland T.J.B. and Powell R. (1998) An internally consistent thermodynamic data set for phases of petrological interest. *Journal of Metamorphic Geology*, **16**, 309–343.

Holland T.J.B. and Powell R. (2009) AX: A program to calculate activities of mineral end-members from chemical analyses.

Karmakar S. (2021) Formation of clinohumite ± spinel in dolomitic marbles from the Makrohar Granulite Belt, Central India: Evidence for Ti mobility during regional metamorphism. *American Mineralogist*, **106**, 1818–1827.

Karmakar S., Mukherjee S., Sanyal S. and Sengupta P. (2017) Origin of peraluminous minerals (corundum, spinel, and sapphirine) in a highly calcic anorthosite from the. *Contributions to Mineralogy and Petrology*, **172**, 67.

Lang H., Wachter A., Peterson V. and Ryan J. (2004) Coexisting clinopyroxene/spinel and amphibole/spinel symplectites in metatroctolites from the Buck Creek ultramafic body, North Carolina Blue Ridge. *American Mineralogist*, **7**, 20–30.

Menegon L., Pennacchioni G. and Stünitz H. (2006) Nucleation and growth of myrmekite during ductile shear deformation in metagranites. *Journal of Metamorphic Geology*, **24**, 553–568.

Mondal S., Uapadhyay D. and Banerjee A. (2017) The origin of rapakivi feldspar by a fluid-induced coupled dissolution–reprecipitation process. *Journal of Petrology*, **58**, 1393–1418, doi: 10.1093/petrology/egx058

Phillips E.R. (1974) Myrmekite – one hundred years later. *Lithos*, **7**, 181–194.

Phillips E.R. (1980) On polygenetic myrmekite. *Geological Magazine*, **117**, 29–36.

Philpotts A.R. and Ague J.J. (2009) *Principles of Igneous and Metamorphic Petrology*. Cambridge University Press, Cambridge, UK.

Plümper O. and Putnis A. (2009) The complex hydrothermal history of granitic rocks: multiple feldspar replacement reactions under subsolidus conditions. *Journal of Petrology*, **50**, 967–987.

Putnis A. (2002) Mineral replacement reactions: from macroscopic observations to microscopic mechanisms. *Mineralogical Magazine*, **66**, 689–708.

Putnis A. and Austrheim H. (2010) Fluid-induced processes: Metasomatism and metamorphism. *Geofluids*, **10**, 254–269, https://doi.org/10.1111/j.1468-8123.2010.00285.x

Remmert P., Heinrich W., Wunder B., Morales L., Wirth R., Rhede D. and Abart R. (2018) Synthesis of monticellite–forsterite and merwinite–forsterite symplectites in the CaO–MgO–SiO$_2$ model system: influence of temperature and water content on microstructure evolution. *Contributions to Mineralogy and Petrology*, **173**, 1–17.

Roy Choudhury S., Dey A., Mukherjee S., Sanyal S., Karmakar S. and Sengupta P. (2023) On the factors controlling the incorporation of aluminium within titanites: a case study from medium pressure calc-silicate granulites in parts of the East Indian shield. *Mineralogy and Petrology*, **117**, https://doi.org/10.1007/s00710-023-00826-1

Schwantke A. (1909) Die Beimischung von Ca in Kalifeldspat und die Myrmekitbildung. *Centraalblad Mineralogische*, **1909**, 311–316.

Sederholm J.J. (1899) *Über eine archäische Sedimentformation im südwestlichen Finland und ihre Bedeutung für die Erklärung der Entstehungsweise des Grundgebirges*, Vol. 6. Bulletin de la Commission géologique de Finlande, Kupio, Finland.

Simpson C. and Wintsch R.P. (1989) Evidence for deformation-induced K-feldspar replacement by myrmekite. *Journal of Metamorphic Geology*, **7**, 261–275.

Stüwe K. (1997) Effective bulk composition changes due to cooling: a model predicting complexities in retrograde reaction textures. *Contributions to Mineralogy and Petrology*, **129**, 43–52, https://doi.org/10.1007/s004100050322

Torres-Roldan R.L., Garcia-Casco A. and Garcia-Sanchez P.A. (2000) CSpace: An integrated workplace for the graphical and algebraic analysis of phase assemblages on 32-bit wintel platforms. *Computers and Geosciences*, **26**, 779–793.

Touret J.L.R., Santosh M. and Huizenga J.M. (2022) Composition and evolution of the continental crust: Retrospect and prospect. *Geoscience Frontiers*, **13**, 101428.

Tsurumi J., Hosonuma H. and Kanagawa K. (2002) Strain localization due to a positive feedback of deformation and myrmekite-forming reaction in granite and aplite mylonites along the Hatagawa Shear Zone of NE Japan. *Journal of Structural Geology*, **25**, 557–574.

Vernon R.H. (1991) Questions about myrmekite in deformed rocks. *Journal of Structural Geology*, **13**, 979–985.

Vernon R.H. (2004) *A Practical Guide To Rock Microstructure*. Cambridge University Press, Cambridge, UK, https://doi.org/10.1017/CBO9780511807206

Vernon R.H., Williams V.A. and D'arcy W.F. (1983) Grain-size reduction and foliation development in a deformed granitoid batholith. *Tectonophysics*, **92**, 123–145.

Whitney D.L. and Evan B.W. (2010) Abbreviations for names of rock-forming minerals. *American Mineralogist*, **95**, 185–187.

Yuguchi T., Sasao E., Ishibashi M. and Nishiyama T. (2015) Hydrothermal chloritization processes from biotite in the Toki granite, Central Japan: Temporal variations of the compositions of hydrothermal fluids associated with chloritization. *American Mineralogist*, **100**, 1134–1152.

Yuguchi T., Shoubuzawa K., Ogita Y., Yagi K., Ishibashi M., Sasao E. and Nishiyama T. (2019) Role of micropores, mass transfer, and reaction rate in the hydrothermal alteration process of plagioclase in a granitic pluton. *American Mineralogist*, **104**, 536–556.

Yuguchi T., Yuasa H., Izumino Y., Nakashima K., Sasao E. and Nishiyama T. (2022) Micropores and mass transfer in the formation of myrmekites. *American Mineralogist*, **107**, 476–488.